Volume 142 | Number 19 | 7 October 2017 | Pages 3525–3760

Analyst

rsc.li/analyst

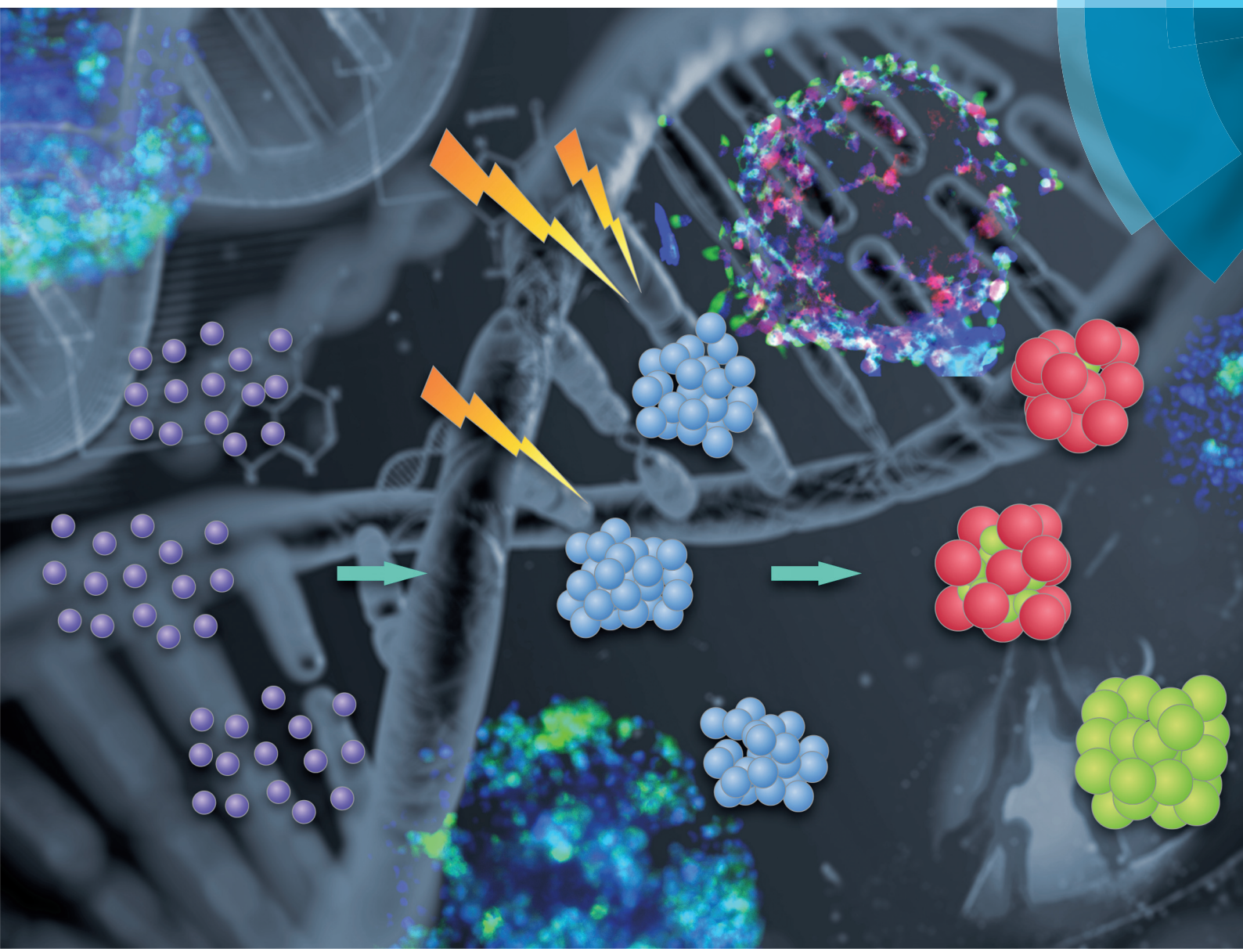

ISSN 0003-2654

ROYAL SOCIETY OF CHEMISTRY

PAPER
Liyuan Ma, Ming Su *et al.*
Three-dimensional microtissues as an *in vitro* model for personalized radiation therapy

Analyst

PAPER

Cite this: *Analyst*, 2017, **142**, 3605

Three-dimensional microtissues as an *in vitro* model for personalized radiation therapy†

Yuting Qiu,[a] Dandan Ning,[b] Peipei Zhang,[b,c] Stephanie Curly,[c] Yong Qiao,[c] Liyuan Ma*[a,b,c] and Ming Su*[a,b]

Received 12th May 2017,
Accepted 26th July 2017

DOI: 10.1039/c7an00794a

rsc.li/analyst

This paper describes the use of 3D microtissues as an intermediate model between the 2D cell culture and the animal model to assess radiation-induced cellular and DNA damage in the context of personalized radiation therapy. An agarose microwell array was used to generate 3D microtissues with controlled size and shape. The microtissues were exposed to X-ray radiation of various doses, and the radiation damage to cells was examined using a variety of techniques with different end points. Damage to cell membranes and reduction in metabolic activity were examined with the MTT assay and dye inclusion assay. DNA damage was tested with the micronucleus assay, γ-H2AX immunostaining, and HaloChip assay. 3D microtissues exposed to X-rays are smaller compared to unexposed ones in extended cultures, indicating that X-ray radiation can retard the growth of cells in 3D microtissues, where cells at the outer shells of microtissues can prevent further damage to those inside.

Introduction

X-ray radiation therapy is used widely to treat localized tumors, and to relieve symptoms of later stage or metastatic cancers.[1–3] A challenge of radiation therapy is that radiation dose under therapeutic conditions can damage normal tissue. This issue is caused by two factors: the selectivity of energy deposition on tumors and the susceptibility of tumors to radiation damage.[4–6] A panel of beam techniques such as image guided radiation therapy and intensity modulated radiation therapy, as well as proton therapy has been used to enhance the energy deposition on tumors to minimize the dose on normal cells and maximize the dose on cancer cells. The radiation beam can be fractionated over space to intersect at tumors from several directions to spare normal cells along the beam path. Multiple beamlets of different intensities can be used to maximize the dose on tumors by conforming to the shape of the tumor. Radiosensitizers such as nanoparticles of heavier elements targeted at the tumor site have been used to enhance the deposition of radiation energy.[7,8] The difference in the repair ability of cancer and normal cells has also been utilized in treatment, where the total radiation dose is fractionated over time to allow normal cells to recover from damage, while cancer cells that are radioresistive in the first period move into a radiosensitive phase of the cell cycle in the next period.[9–11]

Radiosensitivity varies to a great extent across tumor types and between patients bearing the same type of tumor.[12–15] There is a significant need for tools to predict the efficacy of radiation therapy in individual patients.[16–18] The selection of radiation therapy in a treatment plan for a particular patient is driven by the clinical and pathological features of tumors, while the goal of personalized radiation therapy is to identify patients who are sensitive to radiation therapy, where low-risk patients may receive additional benefits from radiation therapy, and high risk ones will be recommended to undergo surgery.[19–21] Meanwhile, this personalized approach can provide alternate dosing schedules for patients to reduce the total radiation dose. The radiosensitivity of a tumor can be assessed by evaluating the gene network through a systems biology approach. Biomarkers derived from tumors can also be used to predict radiation sensitivity, although the prediction outcomes are heterogeneous as a result of gene expression due to epigenetic control.[22–24]

In vitro grown mammalian cells could be readily used to examine the effects of radiation on cancer cells, but cells in two-dimensional (2D) monolayer cultures do not respond to radiation as tissues.[25] More evidence suggests that the 2D monolayer model is not a good representation of the true

[a]*Department of Chemical Engineering, Northeastern University, Boston, MA 02115, USA. E-mail: m.su@northeastern.edu*
[b]*Wenzhou Institute of Biomaterials and Engineering, Wenzhou Medical University, Chinese Academy of Science, Zhejiang 325001, China*
[c]*Department of Biomedical Engineering, Worcester Polytechnic Institute, Worcester, MA 01069, USA*

†Electronic supplementary information (ESI) available. See DOI: 10.1039/c7an00794a

physiological conditions of cancer cells in patients, in which cells are surrounded by and interact through a well-developed extracellular matrix (ECM).[26–28] Other than the geometrical difference, the ECM can regulate almost all cell functions (such as migration and toxicity response), cell mechanics (such as cell stiffness and cell-matrix adhesion), diffusion characteristics (such as drugs, oxygen and free radicals), and abilities to repair damage caused by external stimuli (such as ionizing X-ray radiation and environmental toxins).[29–31] Cells in three dimensional (3D) aggregates are in an environment close to physiological conditions and can mimic the tissue architectures and functions of human beings; meanwhile, these aggregated cells have shown higher stability than those from a 2D culture.[32–35] The cellular functions are well maintained in microtissue cultures, and it is possible that cells in 3D microtissues will have enhanced repair ability or damage tolerance compared to those in the 2D culture, and there is a reduced surface area in 3D microtissues than the 2D cell monolayer. It is believed that 3D tumor microtissue-based toxicity assays can fill the knowledge gap between the *in vitro* 2D cell assay and *in vivo* animal testing.[36–38]

This paper describes the use of 3D microtissues as an intermediate model (between the 2D cell culture and the animal model) to assess radiation induced cellular and DNA damage for personalized radiation therapy (Fig. 1). An agarose microwell array was used to generate 3D microtissues with controlled size and shape. The 3D microtissues are exposed to X-ray radiation of various doses, and the radiation damage to cells is examined at cellular and genetic levels using a variety of techniques. Damage to cell membranes and reduction in metabolic activity are confirmed with the dye inclusion and MTT assay. DNA damage is confirmed with the HaloChip assay, micronucleus assay, and γ-H2AX immunostaining. It is found that 3D microtissues exposed to X-rays are smaller compared to unexposed ones in extended cultures, indicating that X-ray radiation can retard cell growth in 3D microtissues, where cells at the outer shells of microtissues can prevent further damage to those inside.

Experimental

Materials and methods

SYBR GreenER dye was from Invitrogen. Cytokinesis B and agarose (melting temperature of 65 °C) were from VWR. Polyallylamine hydrochloride (PAH, 15 000 Da), polysodium 4-styrene sulfonate (PSS) (70 000 Da), polydiallyl-dimethyl ammonium chloride (PDAC) (100 000–200 000 Da), and rhodamine isothiocyanate (RITC) were from Sigma. Polydimethylsiloxane (PDMS Sylgard 184) was from Dow-Corning. The Vybrant MTT cell proliferation kit, Vybrant cytotoxicity kit, live/dead assay kit, and Quant-iT PicoGreen dsDNA assay kit were from Invitrogen (Carlsbad, CA). RPMI 1640 culture medium, penicillin, streptomycin, fetal bovine serum (FBS), and Dulbecco's phosphate-buffered saline (D-PBS), 4,6-diamidino-2-phenylindole (DAPI), anti-phospho-histone γ-H2AX antibody, and anti-rabbit IgG-FITC antibody were from Sigma (St Louis, MO). HeLa (CLL-2) and MG-63 (CRL-1427) cell lines were from American Type Culture Collection (ATCC, VA).

Three dimensional cell culture

3D microtissues were produced as follows: 50 μL of 2% agarose gel was introduced in each well for 10 min to form a solid non-adhesive agarose gel. Cells were grown in RPMI 1640 medium supplemented with penicillin (100 units per mL) and streptomycin (100 μg mL^{-1}), and 10% fetal bovine serum (FBS) according to the protocol. 20 μL of cell suspension was seeded in each well with a final concentration of 10^5 cells per mL, and the plate was cultured in an incubator with 5% CO_2 at 37 °C to allow microtissues to form on the non-adhesive gel surface.

Microscopy

An inverted optical microscope from Milesco Scientific (AccuScope 3032, Princeton, MN) was used to observe cultured cells. Fluorescence images of microtissues were taken on a Zeiss Axioskop 2 mot plus confocal microscope and an inverted fluorescence microscope from Olympus (GX51). Phase

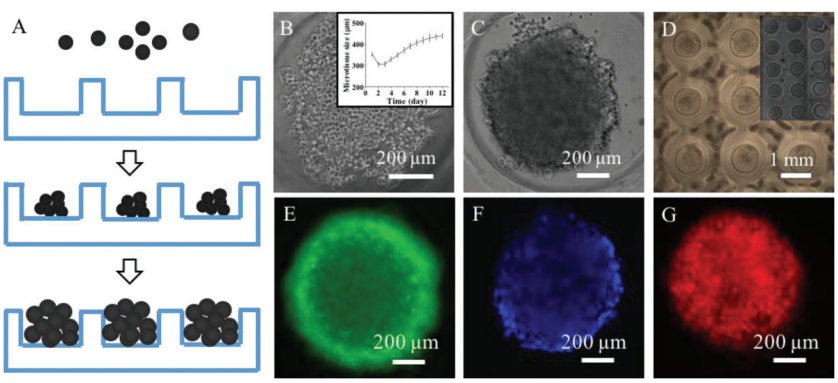

Fig. 1 Predicting the efficacy of radiation therapy with three dimensional (3D) microtissues (A). A phase contrast image of the microtissue composed of HeLa cells (B) and the size of the microtissue as a function of time (inset). Cells tend to grow into a tight 3D structure after 24 h (C). 3D microtissues of the HeLa cells (D), and an enlarged portion of 3D microtissues (inset). Live cells are stained in green in microtissues (E). Fluorescence image of nuclei in microtissues (F). Fluorescence image of microtissues stained with EB (G).

contrast and fluorescence images of cells were taken with Olympus IX 81 or Carl Zeiss (VivaTome) optical microscopes.

X-ray irradiation

A Mini-X X-ray tube (Amptek, Inc., Bedford, MA) operating at a tube voltage of 40 kV and a current of 100 mA is used to generate primary X-rays. The surface dose rate at a distance of 5 cm from the tube is measured with a handheld radiation dosimeter (Mirion RAD-60, Freshwater Systems, Greenville, SC) and is found to be 0.4 Gy h^{-1}. Cells were cultured on coverslips in 6 well plates and exposed to an X-ray (40 kV, 100 μA) for 15 minutes. The 9 × 9 array (surface area of 1 cm^2) of microwells loaded with cells is then fixed at a distance of 5 cm from the X-ray source, which is fitted with a collimator resulting in an output cone angle of 100 for the emerging beam. The X-ray beam covers an area of 2.4 cm^2 on the exposed surface that is sufficient to uniformly irradiate the entire array. All X-ray irradiation experiments are performed inside a radiation shield containing lead sheets to prevent radiation leakage.

Live/dead assays

Calcein AM/EthD-1 (calcein AM and ethidium homodimer) was done as follows. 100 μL of D-PBS was added into each well to wash cells to dilute serum-containing esterase. Then, 100 μL of the dual-fluorescence calcein AM/EthD-1 assay reagent was added into each well, and the plate was incubated for 30 min at room temperature before the fluorescence intensity was measured. A cell free control was used to determine the background fluorescence, which was subtracted before calculation. The percentages of live and dead cells were calculated by the equation provide by the supplier.

MTT assay

MTT[3-(4,5-dimethylthiazol-2-yl)-2,5-diphenyltetrazolium bromide] assay was done as follows. The medium in each well was removed and replaced with 100 μL of fresh medium. 10 microliters of 12 mM MTT stock solution were added into each well and in a negative control (100 μL of medium). After incubation at 37 °C for 4 h, 100 μL of SDS–HCl solution was added into each well and mixed thoroughly by using a pipette. After incubation at 37 °C for 6 h, each sample was mixed well with a pipette and the optical absorbance at 570 nm was recorded using a SpectraMax M3 plate reader (Molecular Devices).

Immunostaining assay

Cells were fixed with 4% paraformaldehyde for 10 min, washed with 0.2% Triton-X 100 in PBS 3 times and incubated at room temperature in PBS containing 1% BSA and 0.2% Triton-X 100 for 1 h. Primary antibodies for the anti-vinculin-FITC antibody were incubated overnight in a blocking buffer at 4 °C. After washing the coverslip the next day, the rabbit secondary antibody was added into it and incubated for 2 h at room temperature. After washing the coverslip, cells were checked with a laser confocal microscope (Zeiss) at 80×.

Micronucleus assay

Microtissues were re-dispersed into discrete cells by using trypsin and pipetting up and down. Cytokinesis B (5 μg ml^{-1}) was added into the cell culture medium. The cells were cultured at 37 °C and 5% CO_2 for 24 h before trypsinization. Cells were then fixed with paraformaldehyde in PBS for 15 min, and treated with 0.1% Triton X-100 in PBS for lysis. Nuclei in cells were stained with DAPI (0.2 μg ml^{-1}, 15 min) and imaged with a fluorescence microscope. The fluorescence intensity is calculated using Image J.

Double strand break

The expression of the DNA repair protein (γ-H2XA) was determined to assess DNA double strand break as follows. Microtissues were re-dispersed into discrete cells by using trypsin and pipetting up and down. The cells were cultured at 37 °C and 5% CO_2 for 30 min, fixed with 4% paraformaldehyde in PBS for 10 min, and treated with 0.1% Triton X-100 in PBS for 5 min. After incubating in blocking buffer (3% bovine serum albumin in PBS) for 1 h, the primary antibody against γ-H2XA was added and incubated at room temperature for 2 h. After rinsing with PBS, the cells were incubated with FITC-washed with PBS. Nuclei of cells were stained with DAPI (0.2 μg mL^{-1}) for 15 min, washed with PBS and observed under a fluorescence microscope.

Apoptosis study

Annexin V conjugated with fluorescein isothiocyanate (FITC) labels phosphatidylserine sites on the membrane surface, and propidium iodide (PI) differentiates apoptotic cells from viable and necrotic cells. Cell apoptosis was examined with the annexin V-FITC/PI kit (BD Biosciences) using flow cytometry. Cells from microtissues were re-suspended in annexin-V binding buffer and cultured with annexin V-FITC/PI in the dark for 15 min. The extent of apoptosis was determined by using a Becton-Dickinson FACScan cytofluorometer (Mansfield). The fraction of cell population in different quadrants was checked by using quadrant statistics. Both early apoptotic (annexin V-positive, PI-negative) and late (annexin V-positive and PI-positive) apoptotic cells were included.

HaloChip assay

Cells from microtissues were patterned to carry out the HaloChip assay as follows. Three layers of a polyelectrolyte (PDAC, PSS and PAH-RITC) were deposited on a PDMS stamp bearing a micropillar array. The stamp was brought into contact with a glass substrate to form an isolated polyelectrolyte array. Cells suspended in the culture medium were incubated on the glass substrate, where the cells were attached on the polyelectrolyte array *via* electrostatic interactions. The attached cells were embedded in agarose gel (0.1% mass), followed by incubating in 0.3 M NaOH for 10 min at room temperature, and staining with 10 μg mL^{-1} SYBR for 10 min. After incubating in deionized water for 3 min to remove excess SYBR, the cells were imaged with fluorescence microscopy.

Statistical analysis

The results were expressed as mean ± standard derivation (SD). The statistical evaluation was performed by Student's *t*-test. $P < 0.05$ was considered statistically significant. The results are denoted with * when $P < 0.05$, and with ** when $P < 0.01$.

Results

Fig. 1A shows the procedure of making 3D cell microtissues, where discrete cells are seeded into and allowed to grow in non-sticky agarose microwells produced with microfabrication. Cells initially seeded in the agarose mold disperse evenly in 2D as shown in Fig. 1B. Cells grow together and form clusters, and the size of microtissues increases as a function of time (Fig. 1B inset). It is observed that the microtissue grows in a typical exponential solid tumor growth pattern during the first few days, followed by a plateau, with little or no growth in the following days. After 24 h, the cells tend to grow into a tight 3D structure (Fig. 1C). Fig. 1D is a phase contrast image of 3D microtissues of HeLa cells placed in an array of microwells.[39,40] A larger area image of 3D microtissues shows that each microtissue has a similar diameter (Fig. 1D inset). In order to determine the viability of cells in the microtissue, the live/dead assay with dual fluorescence staining is carried out with calcein AM/EthD-1, where EthD-1 stains dead cells red by penetrating into membrane damaged cells and combining with DNA in nuclei, and keeps live cells unstained, while calcein AM stains live cells green leaving dead cells unaltered. Fig. 1E shows a fluorescence image of a microtissue where live cells are green. The absence of red color indicates that cells are alive in microtissues. The 3D microtissue shows stronger green color on its edge and weaker color in the center, probably because cells are closely packed and it requires a longer time for the dye to diffuse into the tissue. The nuclei of cells in 3D microtissues are stained with DAPI (Fig. 1F), where the cell nuclei are close to each other, indicating close packing of cells in the microtissues. The nuclei of cells in microtissues are stained using ethidium bromide (EB). Fig. 1G shows a fluorescence image of a single microtissue taken by using a fluorescence microscope under ultraviolet excitation, where DNAs of each cell locate only in the nucleus region. SEM images of 3D microtissues are shown in the ESI.†

The growth dynamics of the microtissues exposed to X-ray radiation is characterized by measuring the diameter of the area covered by microtissues. Fig. 2A1–A3 show the growth of 3D cell microtissues stained with DAPI without X-ray irradiation from day 4 to day 12, respectively, while 2B1–B3 show the growth of 3D microtissues exposed to 10 Gy X-ray from day 4 to day 12, respectively. Fig. 2C1 shows that the size of microtissues increases as a function of time, where 10–12 days of culture can produce uniform HeLa microtissues with an average size of 400 μm, at the initial seeding concentration of 10^5 cells per mL. The microtissue exposed to X-ray follows a similar growth pattern, but the grow rate is lower compared with the non-exposed ones. Fig. 2C2 shows the integrated fluorescence intensities of two samples, where the color intensity of X-ray irradiated microtissues is lower than those of non-irradiated ones. X-ray-induced damage to the nuclei of cells in 400 μm diameter microtissues has been assessed using the micro-nucleus assay. After exposure, the cells in the microtissues were re-dispersed to form isolated cells, and were stained with DAPI. Fig. 2D1–D3 show cells with or without micronuclei, where the cells are irradiated with 1.5 Gy (2D1), with 3 Gy (2D2), and with 15 Gy (2D3) (arrows in 2D1–D3 show micronuclei). The number of micronuclei per 2000 cells is counted as 10, 27 and 59 per 2000 cells for cells exposed to 1.5, 3 and 15 Gy, respectively. In summary, a higher dose of radiation produces more micronuclei, indicating enhanced chromosome damage.

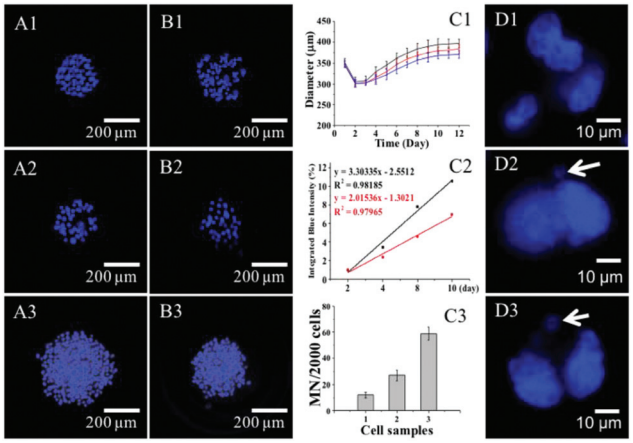

Fig. 2 Fluorescent images of nuclei in microtissues from Day2–Day12 (A1–A3). Fluorescent images of nuclei in microtissues with 10 Gy X-ray irradiation from Day2–Day12 (B1–B3). Growth dynamics of microtissues, microtissues without X-ray irradiation (black line), with 3 Gy (red line), with 15 Gy (blue line). The integrated intensity of fluorescence of two samples, microtissues without X-ray irradiation (black line), with 10 Gy (red line) (C2). The MN number of three samples (C3). Fluorescence image of cells irradiated with 1.5 Gy (D1), with 3 Gy (D2), with 15 Gy (D3).

After X-ray irradiation, trypan blue, a non-fluorescent dye that stains dead cells blue while leaving live cells unaltered, is added into microwells to stain cells in microtissues. Fig. 3A shows a photograph of microwells, where cells are stained with trypan blue after the formation of microtissues. The absence of blue color shows that most cells in microtissues are alive. Fig. 3B and C show the post-irradiation image (0.5 and 1 h) of microtissues that were seeded with the same number of HeLa cells followed by trypan blue staining. The blue color of microtissues in each microwell is clearly visible with the naked eye and the color intensity of the image is proportional to the number of dead cells. Cell viability is monitored for microtissues containing HeLa and MG-63 cells, respectively. This is done by measuring the color intensity of each microwell from images taken every 30 min following a 1 h X-ray exposure (0.4 Gy). Fig. 3D shows that the intensity of blue color increases and saturates to a value of 100 after 9 h; under the same conditions, it takes 12 h for MG-63 cells to reach the same color

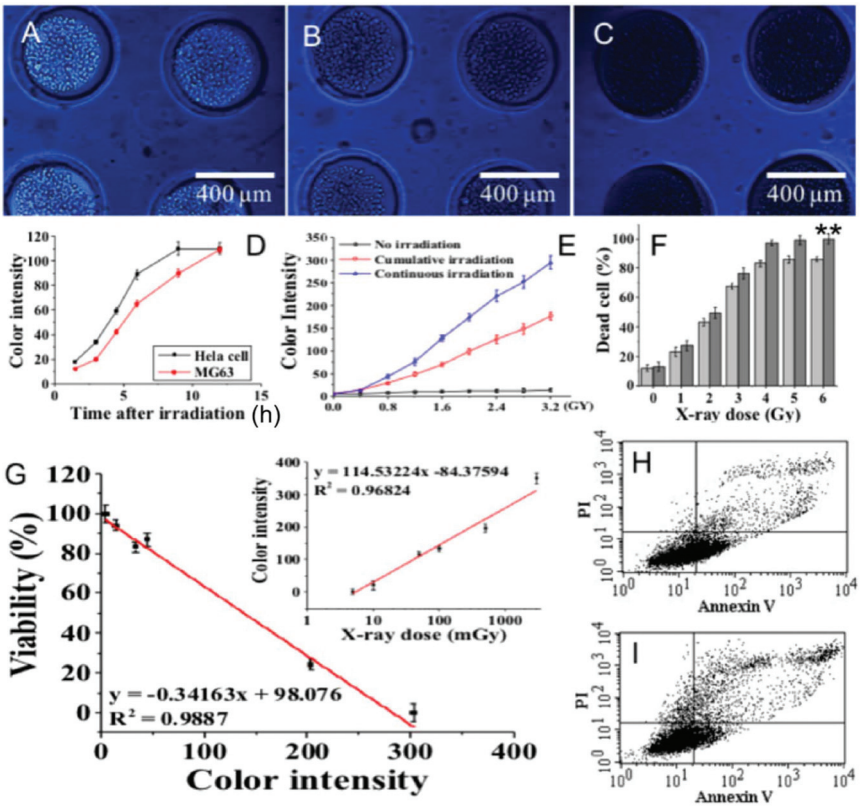

Fig. 3 Optical images of HeLa microtissues in microwells stained with trypan blue, not exposed to X-rays (A), exposed to X-rays for 0.5 h (B) and 1 h (C). The intensity of blue color from trypan blue measured at different times after 1 h X-ray irradiation of microtissues containing different cell lines (D). Color intensity of trypan blue stained HeLa microtissues for continuous and cumulative X-ray exposures (E). Percentage of dead cells for three different cell types after exposure to different X-ray doses (F). HeLa cell viability against the color intensity of trypan blue stain, the inset shows the variation of color intensity for trypan blue stain with X-ray dose (G). Flow cytometry plot of control cells (H), and cells treated with 3 Gy X-ray (I).

intensity. The results confirm that different cell lines respond differently towards the same X-ray dose with HeLa and MG-63 cells being the most and the least sensitive to X-rays, respectively. This can be explained in terms of the difference in the cell cycle: HeLa cells double every 24 h, while MG-63 cells double every 26 h, respectively.[41] After X-ray irradiation, cells do not die until they are in the mitotic period where damaged DNA fails to duplicate. In the case of cumulative exposure, the total dose is fractionated to 1 h per day (0.4 Gy per day) for 8 days, whereas in continuous exposure, the whole dose (3.2 Gy) is applied continuously in one fraction. Fig. 3E shows that the continuous irradiation kills more cells in HeLa microtissues than the cumulative irradiation, especially when the irradiation time is longer than around 3 h. The difference in cumulative and continuous exposures is likely caused by repairing of a small amount of DNA damage. Cumulative exposure provides time for the damaged DNA to be repaired between exposures while in the case of continuous exposure the damage accumulates before it can be repaired in 3D microtissues. Fig. 3F shows the cell death at different radiation doses for two different types of microtissues where the percentage of dead cells correlates with the intensity of trypan blue staining. At higher doses more cells die, resulting in a more intense blue color. The dark grey bar represents HeLa cells; light grey bar represents MG 63. Fig. 3G shows that the increase in the intensity of the blue color is proportional to the decrease in the viability of HeLa microtissues which are monitored with the MTT assay. Similar results are obtained for MG-63 microtissues. The linear relationship between the color intensity and X-ray dose is also plotted accordingly. The limit of detection depends on the cell type, since some cells are more sensitive to radiation than others. Extensive DNA damage can lead to cell apoptosis or death. Flow cytometry was used to determine whether cell death caused by X-ray irradiation was due to apoptosis or necrosis. Annexin V-FITC allows fluorescent detection of annexin V which binds to apoptotic cells. Annexin V conjugated with fluorescein isothiocyanate (FITC) labels phosphatidylserine sites on the cell membrane. Propidium iodide (PI) is added to label cellular DNA in necrotic cells where the cell membrane was compromised. The upper left and lower left quadrants in Fig. 3H show cells that died from apoptosis (Annexin V staining) in the absence of X-rays. In comparison, Fig. 3I shows that the distribution of cells treated with 10 Gy X-ray shifted upward. In the absence of X-ray, among 30% of dead cells, 23.61% were caused by apoptosis. When microtissues are treated with 3 Gy

X-ray, among 50.5% of dead cells, 53.1% are caused by early or late apoptosis. Hence, death in a larger number of cells is caused by apoptosis when treated with X-ray irradiation.

Radiation can destabilize the microtubule network in cells and affect cell migration.[42] Fig. 4A1 shows the extensive microtubule network of untreated cells. This phenomenon correlates with a healthy cell where cargo-carrying motor proteins used the microtubule network to move essential proteins intracellularly. In one of the experiments, cells were treated with 3 Gy X-ray irradiation. Punctate structures form in some cells with 3 Gy of X-ray radiation (Fig. 4B1); Fig. 4A2 shows the extensive microtubule network of untreated cells, disassembly of the microtubule network in most cells can be seen at 3 Gy (Fig. 4B2). Fig. 4A3 and B3 show the merged images of 4A1–4A2 and 4B1–4B2, respectively, while the blue indicates nuclei stained with DAPI. There are less red microtubes with increased X-ray irradiation. The fluorescence integrated intensity of sample 4A3 and sample 4B3 is shown in Fig. 4C, where red and green bars represent α-tubulin and vinculin, respectively. The viabilities of 3D and 2D cells decrease as the X-ray dose increased, the low dose of X-ray radiation shows no significant toxicities on both 3D and 2D cells, and the viability of 3D microtissues is higher than 2D monolayer cells. The reason that 3D microtissues show higher viabilities can be explained by a protective effect of 3D microstructures. Cells at the external surface of microtissues are more susceptible to toxicity than inner cells. The function of individual cells is highly dependent on interactions with 3D organized extracellular matrix (ECM) proteins and neighbouring cells. ECM proteins play important roles in the toxicity tolerance in 3D microtissue cultures because they form a natural barrier that limits the diffusion of the free radicals. Moreover, the cellular functions are well maintained in microtissue cultures, and it is possible that cells in 3D microtissues have enhanced repair ability or damage tolerance compared to those in the 2D culture. The diffusion characteristics are different, for 3D cells, the radiation profile along the radial direction is decreased, while each cell is evenly exposed to the same amount of radiation in 2D cells. The impact of X-ray irradiation on the inner parts of the microtissue is shown in the ESI.†

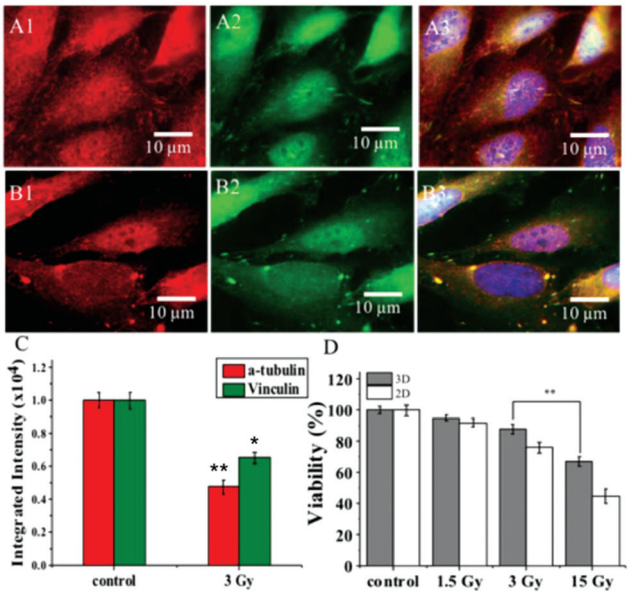

Fig. 4 Fluorescent images of microtubules in cells without X-ray exposure (A1 and A2). Merged fluorescent image (A3). Fluorescent images of microtubules in cells with 3 Gy (B1 and B2). Merged fluorescent image (B3). The integrated intensity fluorescence of three samples (C). Viability of 3D microtissues and 2D cell monolayers after X-ray irradiation (D).

The radiation induced DNA damage has been assessed at a single cell level with the HaloChip assay as follows: 3D microtissues (diameter of 250 μm) with X-ray radiation of 3 Gy and 10 Gy. Cells in the microtissues are re-dispersed by trypsinization to form isolated cells. The single cell array is produced by patterning a positively charged polyelectrolyte multilayer array on the glass substrate. After embedding the arrayed cells in

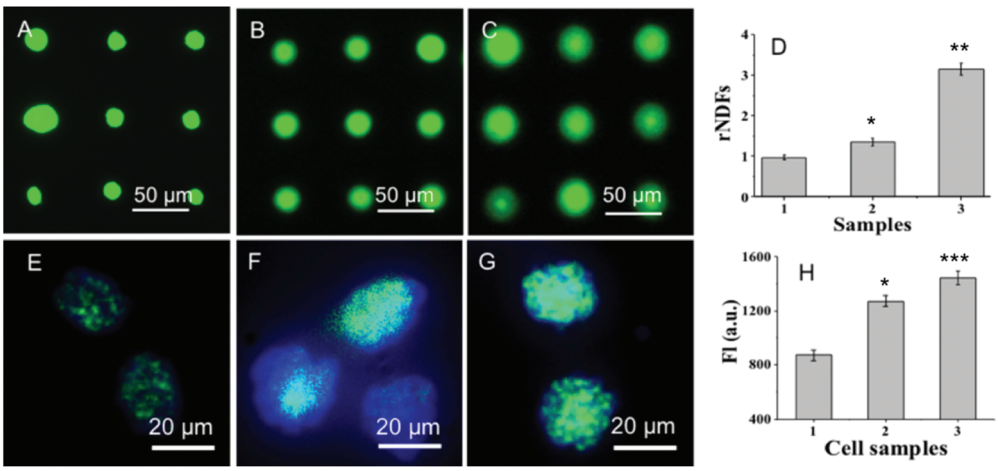

Fig. 5 Halo arrays of cells irradiated with 1.5 Gy (A), 3 Gy (B), and 15 Gy (C). *r*NDF values of the samples (D). Fluorescence images of cells irradiated with 1.5 Gy (E), 3 Gy (F), and 15 Gy (G), and fluorescence intensity of three samples (H).

agarose gel, the sample is immersed in an aqueous solution of NaOH for lysis. Damaged DNA fragments self-diffuse into the gel matrix, and are stained with SYBR green fluorescence dye, forming a diffusive ring around each nucleus. DNA damage is quantified with the relative nuclear diffusion factor (*r*NDF) derived from the areas of halo and the nucleus as follows:

$$r\mathrm{NDF} = (R^2 - r^2)/r^2$$

where R and r are the radio of halo and nucleus, respectively. Fig. 5A–C are halo arrays of three samples: cells irradiated with 1.5 Gy (5A), 3 Gy (5B), and 10 Gy (5C), where the *r*NDF values are shown in Fig. 5D. Sample (1) has smaller *r*NDFs than the other two samples; sample (3) has larger *r*NDFs than sample (2), indicating enhanced DNA damage at a higher dose of X-ray radiation. The X-ray radiation damage to DNA has been assessed at the protein level by measuring the expression of a DNA repair protein, γ-H2AX, which is recruited to the DNA double strand break sites for repair.[42] Cells irradiated with 1.5 Gy show weak green fluorescence (blue is due to DAPI staining of DNA), indicating that a small amount of γ-H2AX is expressed (Fig. 5E). Cells irradiated with 15 Gy radiation show higher γ-H2AX expression than with 3 Gy (Fig. 5G and F), due to the increased dose of radiation. The fluorescence signal from DAPI stained DNA is artificially reduced to highlight green color (Fig. 5E–G). Fig. 5H shows the fluorescence intensities of cells irradiated with (1) 1.5 Gy, (2) 3 Gy, and (3) 15 Gy, where the fluorescence intensity proportionally depends on the radiation dose, confirming the results that more double strand breaks of DNA occur at high radiation doses.

Conclusions

3D microtissues have been generated using agarose microwell arrays with controlled size and shape. 3D microtissues have been used as an intermediate model between the 2D culture and the animal model to assess radiation induced cellular and DNA damage. The radiation damage to cells in 3D microtissues was examined with a variety of techniques with different end points. X-ray irradiation affects differently the growth rate, cell viability and the protein expression of cells in 3D microtissues and the 2D culture. This work has established the way to perform a better radiosensitivity test on patient derived cancer cells to simulate the response of patient during X-ray treatment.

Acknowledgements

This project was supported by a Director's New Innovator Award from the National Institute of Health (1DP2EB016572).

References

1 P. Honkakoski and M. Negishi, *Biochem. J.*, 2000, **347**, 321–337.
2 G. Tarantino, M. N. D. Di Minno and D. Capone, *World J. Gastroenterol.*, 2009, **15**, 2817.
3 G. Luo, T. Guenthner, L.-S. Gan and W. G. Humphreys, *Curr. Drug Metab.*, 2004, **5**, 483–505.
4 N. J. Hewitt, M. J. Gómez Lechón, J. B. Houston, D. Hallifax, H. S. Brown, P. Maurel, J. G. Kenna, L. Gustavsson, C. Lohmann and C. Skonberg, *Drug Metab. Rev.*, 2007, **39**, 159–234.
5 S. Zmora, R. Glicklis and S. Cohen, *Biomaterials*, 2002, **23**, 4087–4094.
6 J. A. DiMasi, R. W. Hansen and H. G. Grabowski, *J. Health Econ.*, 2003, **22**, 151–185.
7 Z. Dereli-Korkut, H. D. Akaydin, A. H. Ahmed, X. Jiang and S. Wang, *Anal. Chem.*, 2014, **86**, 2997–3004.
8 Y. C. Toh, C. Zhang, J. Zhang, Y. M. Khong, S. Chang, D. van Noort, V. Samper, D. W. Hutmacher and H. Yu, *Lab Chip*, 2007, **7**, 302–309.
9 P. S. Dittrich and A. Manz, *Nat. Rev. Drug Discovery*, 2006, **5**, 210–218.
10 B. J. Kane, M. J. Zinner, M. L. Yarmush and M. Toner, *Anal. Chem.*, 2006, **78**, 4291–4298.
11 R. T. Mingoia, D. L. Nabb, C. H. Yang and X. Han, *Toxicol. in Vitro*, 2007, **21**, 165–173.
12 R. Shrivastava, C. Delomenie, A. Chevalier, G. John, B. Ekwall, E. Walum and R. Massingham, *Cell Biol. Toxicol.*, 1992, **8**, 157–170.
13 L. Chan, S. Gosangari, K. Watkin and B. Cunningham, *Apoptosis*, 2007, **12**, 1061.
14 W. Zhou, C. C. Chen, B. Buckland and J. Aunins, *Biotechnol. Bioeng.*, 1997, **55**, 783–792.
15 Y. Torisawa, A. Takagi, Y. Nahimoto, T. Yasukawa, H. Shiku and T. Matsue, *Biomaterials*, 2007, **28**, 559–566.
16 J. Friedrich, R. Ebner and L. A. Kunz-Schughart, *Int. J. Radiat. Biol.*, 2007, **83**, 849–871.
17 W. Zhou, C. C. Chen, B. Buckland and J. Aunins, *Biotechnol. Bioeng.*, 1997, **55**, 783–792.
18 D. Del Duca, T. Werbowetski and R. F. Del Maestro, *J. Neuro-Oncol.*, 2004, **67**, 295–303.
19 F. Pampaloni, E. G. Reynaud and E. H. K. Stelzer, *Nat. Rev. Mol. Cell Biol.*, 2007, **8**, 839–845.
20 C. Y. Li, D. K. Wood, C. M. Hsu and S. N. Bhatia, *Lab Chip*, 2011, **11**, 2967–2975.
21 X. Y. Wang, V. Veerappan, C. Cheng, X. Jiang, R. D. Allen, P. K. Dasgupta and S. R. Liu, *J. Am. Chem. Soc.*, 2010, **132**, 40–41.
22 G. H. Lee, J. S. Lee, X. Wang and S. H. Lee, *Adv. Healthcare Mater.*, 2016, **5**, 56–74.
23 K. H. Nam, A. S. Smith, S. Lone, S. Kwon and D. H. Kim, *J. Lab. Autom.*, 2015, **20**, 201–215.
24 V. S. Repin, I. N. Saburina, N. V. Kosheleva, A. A. Gorkun, I. M. Zurina and A. A. Kubatiev, *Bull. Exp. Biol. Med.*, 2014, **158**, 137–144.
25 J. Y. Kim, D. A. Fluri, R. Marchan, K. Boonen, S. Mohanty, P. Singh, S. Hammad, B. Landuyt, J. G. Hengstler, J. M. Kelm, A. Hierlemann and O. Frey, *J. Biotechnol.*, 2015, **205**, 24–35.

26 F. Brochard and P. G. Degennes, *J. Chem. Phys.*, 1977, **67**, 52–56.
27 H. Zhu, S. Mavandadi, A. F. Coskun, O. Yaglidere and A. Ozcan, *Anal. Chem.*, 2011, **83**, 6641.
28 A. P. Rago, D. M. Dean and J. R. Morgan, *Biotechnol. Bioeng.*, 2009, **102**, 1231–1241.
29 H. Ota, R. Yamamoto, K. Deguchi, Y. Tanaka, Y. Kazoe, Y. Sato and N. Miki, *Sens. Actuators, B*, 2010, **147**, 359.
30 W. Wang, K. Itaka, S. Ohba, N. Nishiyama, U. I. Chung, Y. Yamasaki and K. Kataoka, *Biomaterials*, 2009, **30**, 2705.
31 L. Just, A. Kursten, T. Borth-Bruhns, W. Lindenmaier, M. Rohde, K. Dittmar and A. Bader, *Dev. Dyn.*, 2006, **235**, 2200.
32 R. A. Walters and D. F. Petersen, *Biophys. J.*, 1968, **8**, 1475.
33 T. Straume, J. N. Lucas, J. D. Tucker, W. L. Bigbee and R. G. Langlois, *Health Phys.*, 1992, **62**, 122.
34 C. A. Sevilla, D. Dalecki and D. C. Hocking, *Tissue Eng.*, 2010, **16**, 3805–3819.
35 C. E. Redon, A. J. Nakamura, K. Gouliaeva, A. Rahman, W. F. Blakely and W. M. Bonner, *PLoS One*, 2010, **5**, e15544.
36 A. Vral, M. Fenech and H. Thierens, *Mutagenesis*, 2011, **26**, 11.
37 S. A. Amundson, M. Bittner, P. Meltzer, J. Trent and A. J. Fornace Jr., *Expert Rev. Mol. Diagn.*, 2001, **1**, 211.
38 Y. S. Kim and M. D. Morris, *Anal. Chem.*, 1995, **67**, 784–786.
39 M. B. Grace, B. R. Moyer, J. Prasher, K. D. Cliffer, N. Ramakrishnan, J. Kaminski, C. N. Coleman, R. G. Manning, B. W. Maidment and R. Hatchett, *Health Phys.*, 2010, **98**, 172.
40 C. Y. Li, D. K. Wood, C. M. Hsu and S. N. Bhatia, *Lab Chip*, 2011, **11**, 2967.
41 R. Zhao, C. Chen and D. H. S. Reich, *Biomaterials*, 2014, **35**, 5056–5064.
42 Y. Qiao, C. Wang, M. Su and L. Ma, *Anal. Chem.*, 2012, **84**, 1112–1116.